Nuclear structure of the first 2^+ state in radioactive ^{68}Ge based on g factor and lifetime measurements

J. Leske, K.-H. Speidel, S. Schielke, and O. Kenn

Helmholtz-Institut für Strahlen- und Kernphysik, Universität Bonn, Nussallee 14-16, D-53115 Bonn, Germany

J. Gerber

Institut de Recherches Subatomiques, F-67037 Strasbourg, France

P. Maier-Komor

Physik-Department, Technische Universität München, James-Franck-Strasse, D-85748 Garching, Germany

S. J. Q. Robinson

Geology and Physics Department, University of Southern Indiana, Evansville, Indiana 47712

A. Escuderos, Y. Y. Sharon, and L. Zamick

Department of Physics & Astronomy, Rutgers University, Piscataway, New Jersey 08855

The g factor of the 2_1^+ state of radioactive ^{68}Ge ($T_{1/2} = 270$ d) has been measured for the first time. The technique used is based on α transfer from a ^{12}C target to energetic ^{64}Zn projectiles that incorporates the favorable conditions of inverse kinematics as in projectile Coulomb excitation. It also includes features of the transient field technique applied to nuclear spin precessions. Because the reaction cross section is large the method is a significant alternative to Coulomb excitation of low-intensity radioactive ion beams. In addition, we have remeasured the lifetimes of several excited states using the Doppler-shift-attenuation method. In these measurements, the inherent focusing nature of the reaction in the forward direction was optimally exploited for the resulting fast-moving nuclei. The g factor value obtained, $g(2_1^+) = +0.55(14)$, is in good agreement with the collective value, $g = Z/A = 0.47$, and is also consistent with the precise data of the stable even-A Ge isotopes. The newly determined lifetimes partially agree with those quoted in the literature and are of comparable accuracy. The deduced $B(E2)$ values and the new measured g factor are well reproduced by some fp shell model calculations in which excitations from the $f_{7/2}$ orbital play an important role.

I. INTRODUCTION

The nucleus ^{68}Ge has four protons and eight neutrons outside the doubly magic ^{56}Ni core. In the valence configuration shell model space the possible active orbitals are those of the $N = 3$ $p_{3/2}$, $f_{5/2}$, and $p_{1/2}$ subshells and of the $N = 4$ $g_{9/2}$ intruder subshell.

When one tries to understand the properties of the low-lying states of ^{68}Ge in terms of the spherical shell model, several interesting questions arise: What is the role of core excitations from the $f_{7/2}$ proton and neutron subshells? Can the $g_{9/2}$ orbital be excluded from consideration? Can the simpler shell model picture (with only the $p_{3/2}$, $f_{5/2}$, and $p_{1/2}$ orbitals active) account for any observed collective effects?

For nuclei in this region the answers to these questions depend on the numbers of valence protons and neutrons outside the ^{56}Ni core, as was shown by Honma *et al.* [1,2]. For the Ni isotopes [3–5] and the light Zn isotopes [6] excitations from the $f_{7/2}$ core have been shown to be important. In particular for the Ni isotopes, the positive sign of the measured g factors of the 2_1^+ states as well as the magnitude and the variation with neutron number of the experimental $B(E2)$ values could only be explained by considering strong excitations of the ^{56}Ni core. In contrast, for some of the heavier Zn isotopes, a closed ^{56}Ni

core, but with the indispensable inclusion of the $g_{9/2}$ orbital, was found to be sufficient to explain some of the data fairly well [7].

The explanation of the superdeformation in an excited band recently observed in ^{68}Ge invoked excitations of two $f_{7/2}$ protons [8]. In contrast, the states of this nucleus with low spins and low excitation energies can be well described in the fpg valence space by assuming an inert ^{56}Ni core [8]. Evidently, in this latter situation, the breaking of the ^{56}Ni core becomes energetically more costly.

In an effort to answer some of these questions, the present work focuses on more detailed spectroscopic information for some low-lying levels in ^{68}Ge. The g factor of the 2_1^+ state and the lifetime of the 2_3^+ state were both measured for the first time, and the 2_1^+, 2_2^+, and 4_1^+ lifetimes have been remeasured. The experimental results are interpreted in terms of shell model calculations.

Owing to the lack of a *radioactive* ^{68}Ge beam for Coulomb excitation of the 2_1^+ state, we have used a different technique that had been already successfully applied, for similiar investigations, to the radioactive ^{44}Ti [9] and ^{62}Zn [6] nuclei. This technique is based on α transfer from a light mass target nucleus to a heavy-mass stable beam. It incorporates

the advantages of inverse kinematics, namely strong focusing of the resulting nuclei in the beam direction, just as in projectile Coulomb excitation experiments. The α-transfer reaction from a carbon target is particularly strong and rather selective with respect to the state of interest: The 2_1^+ state is predominantly populated and its feeding from higher lying states is rather weak and therefore practically negligible. This feature is very important for a meaningful measurement of the 2_1^+ state since the feeding corrections to the observed precession, which are indispensable in fusion reactions, can be ignored (see subsequent discussion). Altogether, the transfer reaction provides favorable conditions both for the transient field technique in the measurement of the g factor and also for the Doppler-shift-attenuation method (DSAM) for determining the nuclear lifetime.

II. EXPERIMENTAL DETAILS

In the experiment, a beam of isotopically pure ^{64}Zn ions was accelerated to an energy of 180 MeV at the Munich tandem accelerator, providing intensities of (10–20) enA on a multi-layered target. For these conditions the ion source delivered ZnO$^-$ ions with high intensity for first-stage acceleration onto the stripper.

The target consisted of 0.50 mg/cm^2 of natural carbon deposited on 3.26 mg/cm^2 Gd, which was evaporated on a 1.8 mg/cm^2 Ta foil, backed by a 4.25 mg/cm^2 Cu layer. For the Gd evaporation the same procedure was applied to achieve the optimum magnetic properties [10], which generally resulted in a saturation magnetization close to the theoretical value [11]. Besides the Coulomb excitation of the ^{64}Zn projectiles in inelastic collisions with carbon nuclei [6], strong α transfer occurred in the ^{12}C(^{64}Zn, ^{8}Be)^{68}Ge reaction, whereby the ^{68}Ge(2_1^+) state was predominantly populated. The relevant level scheme of ^{68}Ge is shown in Fig. 1 [12]. The residual nuclei, ^{64}Zn and ^{68}Ge from Coulomb excitation and α transfer, respectively, both move through the Gd layer for spin precession and are stopped in the hyperfine interaction-free environment of the Cu layer.

The deexcitation γ rays of ^{68}Ge were measured in coincidence with forward-emitted α particles from the decay of ^{8}Be, which were detected in a 100 μm Si counter placed at 0° relative to the beam axis. A Ta foil between the target and detector served as a beam stopper, which was, however, transparent for the relevant particles, α's and carbon ions. The latter were used in coincidence for the spectroscopy of Coulomb excited ^{64}Zn, which will be discussed in a forthcoming paper [7]. The Si detector was operated with an exceptionally low bias of ∼3 V. This enabled a better separation in energy of the α particles from the carbon ions owing to their different stopping behavior in the reduced depletion layer of the detector. The same procedure was applied in former measurements with equally good results [6,9].

Two 12.7 cm × 12.7 cm NaI(Tl), and two 9-cm × 9-cm BaF$_2$ scintillators have been used for γ detection and were placed in pairs symmetric to the beam direction. An intrinsic Ge detector with a relative efficiency of 40% served as a
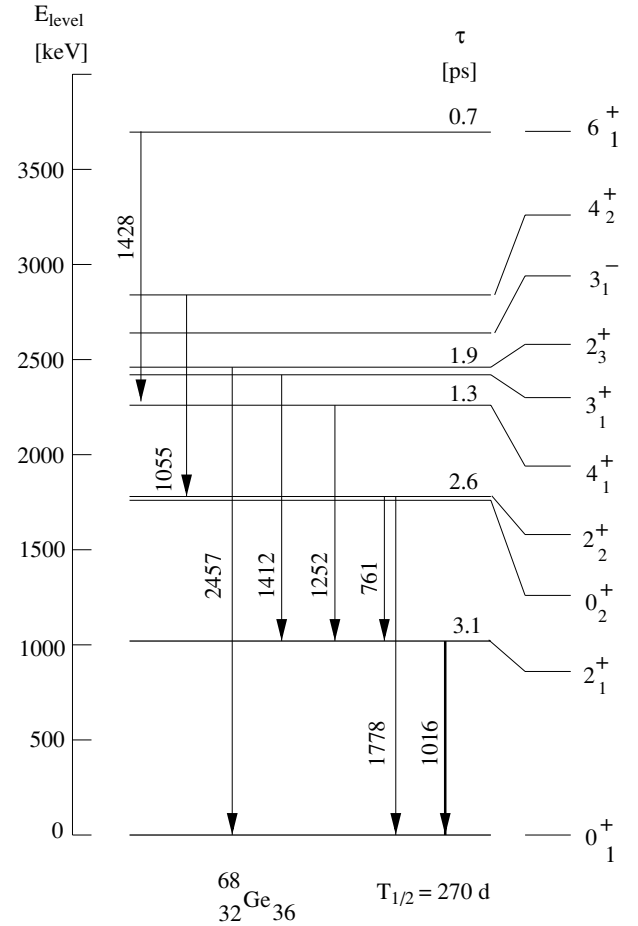

FIG. 1. Level scheme with relevant γ transitions. The lifetimes of the 2_1^+, 4_1^+, 2_2^+, and 2_3^+ states are results of the present work (see text).

monitor for contaminant lines in the ($2_1^+ \rightarrow 0_1^+$) energy region of the γ spectra. Because of its superior energy resolution it was possible to measure the characteristic Doppler-broadened line shapes of several γ transitions, thus enabling the deduction of the nuclear lifetimes. For this purpose the detector was placed at 0°. In Fig. 2 a typical coincident γ spectrum of the Ge detector is displayed, with a window setting on the α-particle channel and low background from the carbon ions (associated with the excitation of ^{64}Zn). As seen from the figure, the spectrum shows practically only the γ lines of ^{68}Ge (with a small contribution from the ^{64}Zn($2_1^+ \rightarrow 0_1^+$) transition), among which the ($2_1^+ \rightarrow 0_1^+$) at 1016 keV is the most prominent line.

Detailed ($2\alpha - \gamma$) angular correlations $W(\Theta_\gamma)$ have been measured for determining the slope $|S| = [1/W(\Theta_\gamma)][dW(\Theta_\gamma)/d\Theta_\gamma]$ in the rest frame of the γ-emitting nuclei at $\Theta_\gamma^{\text{lab}} = \pm 65°$, where the sensitivity to the precession is optimal. Precession angles were derived from counting-rate ratios R for "up" and "down" directions of the external magnetizing field and can be expressed as [4]

$$\Phi^{\text{exp}} = \frac{1}{S}\frac{\sqrt{R}-1}{\sqrt{R}+1} = g\frac{\mu_N}{\hbar}\int_{t_{\text{in}}}^{t_{\text{out}}} B_{\text{TF}}[v_{\text{ion}}(t)]e^{-\frac{t}{\tau}}dt, \quad (1)$$
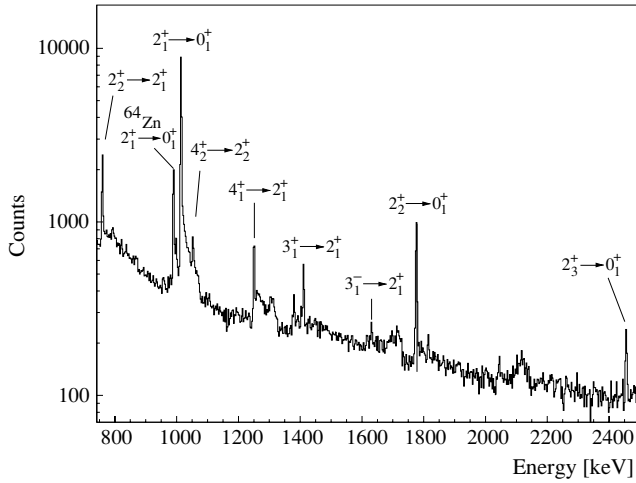
FIG. 2. γ-coincidence spectrum of ^{68}Ge observed with the $0°$ Ge detector gated with the two α particles of the transfer reaction. The Doppler-broadened line shapes reflect the nuclear lifetimes.

where g is the g factor of the 2_1^+ state. Here B_{TF} is the velocity-dependent transient field acting for the time interval $(t_{out} - t_{in})$ that the ions spend in the Gd layer; the exponential accounts for the decay of the excited state during its lifetime τ.

Corrections to the 2_1^+ precession caused by feeding and contaminant admixtures in the photo peak intensity of the scintillator spectra have been considered. The main feeding components are associated with the decay of the 4_1^+ state and the 2_2^+ state, each contributing with a relative intensity of $\simeq 10\%$. Assuming the same g factors for all three states in question and including the observed vanishingly small slope of the $(2_2^+ \to 2_1^+)$ angular correlation, one obtains a change of $\simeq 3\%$ in the 2_1^+ precession (see also [13]). The contaminant admixture in the $(2_1^+ \to 0_1^+)$ γ-line intensity was estimated to be less than 8%. Hence, both effects can be neglected in view of the accuracy ascribed to the measured $g(2_1^+)$ value.

The lifetimes of the states in question were redetermined from the measured line shapes of the corresponding γ lines using the DSAM technique. In the analysis, using the computer code LINESHAPE [14], the Doppler-broadened line shapes were fitted for the reaction kinematics, by applying stopping powers [15] to Monte Carlo simulations including the second-order Doppler effect as well as the finite size and energy resolution of the Ge detector. Feeding from higher states was also included.

III. RESULTS AND DISCUSSION

The g factor of the 2_1^+ state was derived from the measured precession angle Φ^{exp} by determining the effective transient field on the basis of the empirical linear parametrization [3]

$$B_{TF}(v_{ion}) = G_{beam} \cdot B_{lin} \tag{2}$$

with

$$B_{lin} = a(Gd) \cdot Z_{ion} \cdot (v_{ion}/v_0). \tag{3}$$

Here the strength parameter $a(Gd) = 17(1)$T, $v_0 = e^2/\hbar$, and $G_{beam} = 0.61(6)$ is the attenuation factor of the transient field strength induced by the Zn beam in the Gd layer. The values quoted for $a(Gd)$ and G_{beam} refer to the present experimental conditions. The strength parameter of the transient field is based on numerous data using evaporated Gd layers [10]. The attenuation factor G_{beam} was obtained from systematics based on the energy loss of the Zn beam ions in Gd and the velocity of the nuclear excited Zn ions. Previously, this procedure has been carefully and successfully applied to numerous precession data, demonstrating its high reliability (see also [17]).

The precession and lifetime data, together with the deduced g factor of the 2_1^+ state in ^{68}Ge, are summarized in Table I. Evidently, the newly determined lifetimes of the 2_1^+ and 4_1^+ states agree, within their experimental uncertainties, with those of the literature [12]; the average values were included in the table. A large discrepancy, however, exists for the 2_2^+ state, where the new lifetime is considerably shorter. The present value was determined from the line shapes of the $(2_2^+ \to 2_1^+)$ and the $(2_2^+ \to 0_1^+)$ transitions, both of which yielded consistent results. For the analysis the different backgrounds at low and high energies in the spectrum have been carefully examined with respect to contaminant lines. It is noted that the longer 2_2^+ lifetime value, with which the present value disagrees, was obtained in 1977 by Gusinskii *et al.* [18] in an early recoil-distance measurement employing a fusion reaction and γ-singles spectroscopy. The procedure and data analysis of that time involve, from the perspective of present-day knowledge, many uncertainties, which cast doubt on the reliability of this result. The lifetime of the 2_3^+ state is completely new. The $B(E2)$ values deduced from the lifetimes are summarized in Table II.

The $g(2_1^+)$ factor has been compared to the $g(2_1^+)$ values of all the stable even-A Ge isotopes [16]. As shown in Fig. 3, all these data follow nicely the prediction of the hydrodynamical model, with $g = Z/A$. This observation is not surprising since

TABLE I. Summary of the slope of the measured angular correlation, the experimental precession angle, and the deduced g factor and lifetimes. Comparisons are made to earlier data [12].

E_x (MeV)	τ (ps)			$|S(65°)|$	Φ^{exp} (mrad)	$g(2_1^+)$
	[12]	present	average			
2_1^+: 1.016	2.6(3)	3.1(2)	2.9(2)	0.399(38)	15.4(3.5)	+0.55(14)
2_2^+: 1.778	6.1(10)	2.6(2)	—	—	—	—
4_1^+: 2.268	1.2(1)	1.3(2)	1.2(1)	—	—	—
2_3^+: 2.457	—	1.9(6)	—	—	—	—

TABLE II. Experimental energies, $B(E2)$'s, and $g(2_1^+)$ for ^{68}Ge in comparison with results from fp shell model calculations using the FPD6 effective interaction and several shell model spaces. The symmetrized errors of the $B(E2)$'s include the uncertainties of the measured lifetimes and branching as well as mixing ratios taken from [12]. FPD6(t) refers to an FPD6 calculation in which up to t particles could be excited from the $f_{7/2}$ orbital into the $(p_{3/2}, f_{5/2}, p_{1/2})$ space. The collective model predicts $g(2_1^+) = Z/A = 0.47$ (see text).

Quantity	Experimental	FPD6(0)	FPD6(2)	FPD6(4)	FPD6(10)
$E(2_1^+)$ (MeV)	1.016	0.929	0.960	0.945	0.944
$E(2_2^+)$ (MeV)	1.778	1.520	1.547	1.537	1.539
$E(0_2^+)$ (MeV)	1.755	1.708	2.114	2.255	2.269
$E(4_1^+)$ (MeV)	2.268	1.613	1.843	1.915	1.923
$E(3_1^+)$ (MeV)	2.428	2.034	2.163	2.191	2.196
$E(2_3^+)$ (MeV)	2.457	2.098	2.492	2.586	2.595
$E(4_2^+)$ (MeV)	2.833	1.935	2.095	2.161	2.169
$E(6_1^+)$ (MeV)	3.696	2.766	3.142	3.311	3.328
$g(2_1^+)$	+0.55(14)	+0.527	+0.633	+0.633	+0.631
$B(E2; 0_1^+ \rightarrow 2_1^+)$ (e^2b^2)	0.130(9)	0.1239	0.1833	0.2037	0.2054
$B(E2; 2_1^+ \rightarrow 4_1^+)$ (e^2b^2)	0.040(3)	0.0001	0.0048	0.0165	0.0180
$B(E2; 0_1^+ \rightarrow 2_2^+)$ (e^2b^2)	0.0027(3)	0.0013	0.0003	0.00001	0.0000
$B(E2; 2_1^+ \rightarrow 2_2^+)$ (e^2b^2)	0.0019(9)	0.0250	0.0489	0.0543	0.0546
$B(E2; 0_1^+ \rightarrow 2_3^+)$ (e^2b^2)	0.0012(4)	0.0009	0.0013	0.0020	0.0020
$B(E2; 2_1^+ \rightarrow 4_2^+)$ (e^2b^2)	0.0013(8)	0.0422	0.0682	0.0706	0.0699
$B(E2; 4_1^+ \rightarrow 6_1^+)$ (e^2b^2)	0.029(8)	0.0149	0.0259	0.0312	0.0317

the *even–even* Ge isotopes have been generally discussed in the context of vibrational models [19].

We now have much more experimental information on the nuclear structure of ^{68}Ge than was discussed in [19] and [20]. It is worthwhile to note that the data do correspond fairly well to many of the features expected for a vibrational nucleus. The $g(2_1^+)$ of +0.55(14) is consistent with the Z/A

prediction of +0.47. The 2_2^+ and 0_2^+ energies (Fig. 1) differ only by 23 keV. The centroid of the excitation energies of the two-phonon triplet—2_2^+ (1.778 MeV), 0_2^+ (1.755 MeV), and 4_1^+ (2.268 MeV)—is at 2.070 MeV [20], at approximately twice the energy of the 2_1^+ state, as expected. Moreover, the $B(E2; 0_1^+ \rightarrow 2_1^+)$ of $\simeq$15 W.u. significantly exceeds single particle estimates (see Table II). The experimental
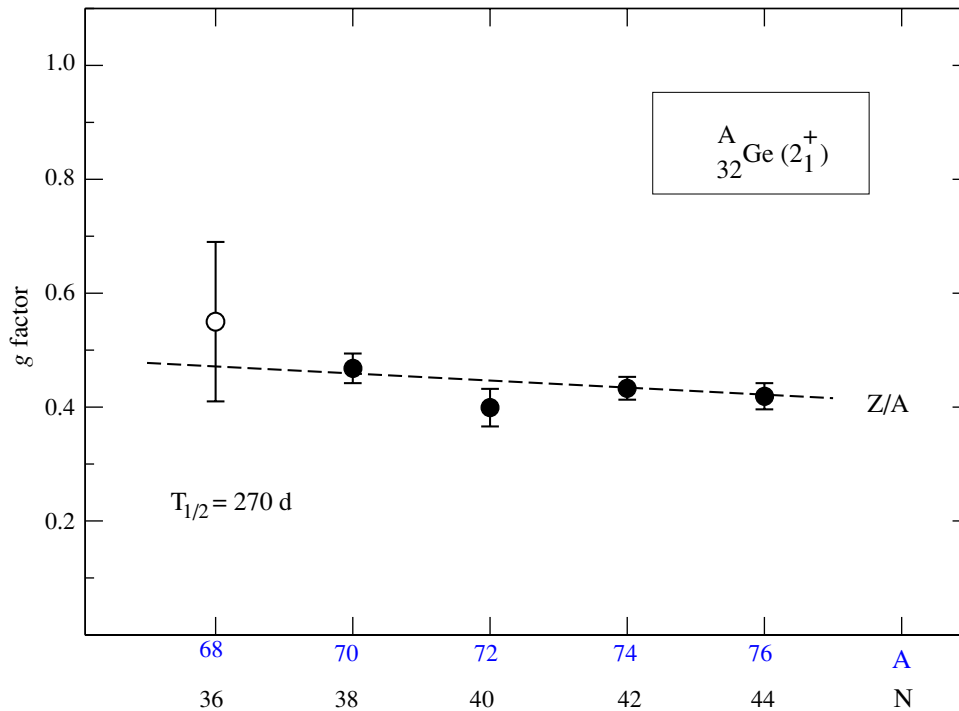

FIG. 3. (Color online) Experimental g factors of the 2_1^+ states of the even-A Ge isotopes as a function of mass and neutron number. The present result for ^{68}Ge (open circle) is compared with stable neutron-rich isotopes [16] (closed circles). The dashed line exhibits the prediction Z/A of the hydrodynamical model.

TABLE III. Experimental energies, $B(E2)$'s, and $g(2_1^+)$ for ^{68}Ge in comparison with results from fp shell model calculations using the GXPF1 effective interaction and several shell model spaces. The symmetrized errors of the $B(E2)$'s include the uncertainties of the measured lifetimes and branching as well as mixing ratios taken from [12]. GXPF1(t) refers to an GXPF1 calculation in which up to t particles could be excited from the $f_{7/2}$ orbital into the $(p_{3/2}, f_{5/2}, p_{1/2})$ space. The collective model predicts $g(2_1^+) = Z/A = 0.47$ (see text).

Quantity	Experimental	GXPF1(0)	GXPF1(2)	GXPF1(4)	GXPF1(10)
$E(2_1^+)$ (MeV)	1.016	1.156	1.198	1.175	1.173
$E(2_2^+)$ (MeV)	1.778	2.084	1.841	1.814	1.814
$E(0_2^+)$ (MeV)	1.755	2.128	1.753	1.713	1.712
$E(4_1^+)$ (MeV)	2.268	2.029	2.472	2.490	2.487
$E(3_1^+)$ (MeV)	2.428	2.655	2.372	2.331	2.331
$E(2_3^+)$ (MeV)	2.457	2.439	2.437	2.378	2.375
$E(4_2^+)$ (MeV)	2.833	2.806	2.559	2.574	2.580
$E(6_1^+)$ (MeV)	3.696	4.339	4.115	4.035	4.032
$g(2_1^+)$	+0.55(14)	+0.543	+0.459	+0.461	+0.462
$B(E2; 0_1^+ \rightarrow 2_1^+)$ (e^2b^2)	0.130(9)	0.0515	0.1118	0.1296	0.1307
$B(E2; 2_1^+ \rightarrow 4_1^+)$ (e^2b^2)	0.040(3)	0.0024	0.0015	0.0667	0.0676
$B(E2; 0_1^+ \rightarrow 2_2^+)$ (e^2b^2)	0.0027(3)	0.0037	0.0017	0.0008	0.0008
$B(E2; 2_1^+ \rightarrow 2_2^+)$ (e^2b^2)	0.0019(9)	0.0069	0.0285	0.0345	0.0348
$B(E2; 0_1^+ \rightarrow 2_3^+)$ (e^2b^2)	0.0012(4)	0.0086	0.0052	0.0043	0.0043
$B(E2; 2_1^+ \rightarrow 4_2^+)$ (e^2b^2)	0.0013(8)	0.0205	0.0568	0.0026	0.0027
$B(E2; 4_1^+ \rightarrow 6_1^+)$ (e^2b^2)	0.029(8)	0.0038	0.00004	0.0748	0.0758

$B(E2; 0_1^+ \rightarrow 2_2^+)$ is smaller by a factor of about 50 than the experimental $B(E2; 0_1^+ \rightarrow 2_1^+)$. However, the measured ratio $B(E2; 2_1^+ \rightarrow 4_1^+)/B(E2; 0_1^+ \rightarrow 2_1^+)$ is about 0.3 whereas the vibrational prediction is 0.72.

In view of the present new data one would like to understand the low-energy structure of ^{68}Ge in terms of the spherical shell model. For these calculations, based on an inert core plus valence nucleons in the fp shell model space (and excluding the $g_{9/2}$ orbital), the shell model codes OXBASH [21] and ANTOINE [22] have been utilized. The extensive calculations of [1,2] concentrated mostly on nuclei with A < 67. Our calculations for $A = 68$ utilized two interactions that have been commonly applied to nuclei in the fp shell: FPD6 [23] and GXPF1 [1,2].

The FPD6 interaction has been extensively used for a long time to explain properties of fp shell nuclei, especially in the lower fp shell. The GXPF1 interaction was developed more recently to also account for properties of nuclei heavier than ^{56}Ni and to easily enable consideration of particle-hole excitations from the ^{56}Ni core. Both interactions involve A-scaling for the two-body matrix elements.

The simplest shell model picture for $^{68}_{32}$Ge$_{36}$ would involve closed proton and neutron $f_{7/2}$ and $p_{3/2}$ subshells, corresponding to an inert ^{64}Ge ($N = Z = 32$) core, with four valence neutrons in the $(f_{5/2}, p_{1/2})$ space. For both interactions this simple picture is inadequate to explain the overall experimental data, since the calculated $B(E2)$'s are typically 5–40 times smaller than the experimental ones. However, the g factor of the $(f_{5/2})^n$ neutron configuration is +0.547 for any n, the Schmidt value of a $f_{5/2}$ neutron, which agrees with the experimental value.

We next considered a larger space, consisting of a closed $f_{7/2}$ shell in both protons and neutrons. This corresponds to an inert ^{56}Ni core plus four valence protons and eight neutrons occupying the $p_{3/2}$, $f_{5/2}$, and $p_{1/2}$ orbitals. The results of the

calculations in this space are given in the FPD6(0) column in Table II and in the GXPF1(0) column in Table III. Here the (t) notation indicates a $(p_{3/2}, f_{5/2}, p_{1/2})$ model space with a maximum number of t nucleons excited from the $f_{7/2}$ orbital. All the calculations utilized $e_\pi = 1.5$, $e_\nu = 0.5$, $g(s)_\pi = 5.586$, $g(s)_\nu = -3.826$, $g(l)_\pi = 1$, and $g(l)_\nu = 0$. We see that with $t = 0$ both interactions give nearly identical results for the $g(2_1^+)$; the excitation energies are better with GXPF1(0); neither interaction adequately explains the $B(E2)$'s, often underestimating them. In subsequent calculations the (0) space [i.e. the $(p_{3/2}, f_{5/2}, p_{1/2})$ space] was expanded to allow also the excitation of up to t nucleons from the $f_{7/2}$ subshell in the ^{56}Ni core to the $(p_{3/2}, f_{5/2}, p_{1/2})$ space. The results are summarized in Tables II and III, where we are trying to explain sixteen experimental numbers.

It is noted, by comparing GXPF1(4) and GXPF1(10), or FPD6(4) and FPD6(10), that very little additional impact is obtained by permitting the excitation of additional $f_{7/2}$ nucleons beyond $t = 4$. Indeed, for both interactions excellent convergence with t, for all quantities, occurs for $t = 4$. The excitation energies obtained are overall quite near the experimental ones for GXPF1(4). For every column in Tables II and III the $g(2_1^+)$ agrees with the measured value within the experimental error. For both interactions the $g(2_1^+)$ value changes by 15%–20% in going from $t = 0$ to $t = 2$ and stays essentially constant from $t = 2$ to $t = 4$.

For the $B(E2)$'s, GXPF1(4) does better than the GXPF1(0) or the FPD6(4) in explaining the experimental data. The experimental $B(E2)$'s are largest for the yrast transitions $0_1^+ \rightarrow 2_1^+$, $2_1^+ \rightarrow 4_1^+$, and $4_1^+ \rightarrow 6_1^+$, and so are the corresponding $B(E2)$'s in GXPF1(4). It is further interesting to compare $B(E2; 2_1^+ \rightarrow 4_1^+)$ and $B(E2; 2_1^+ \rightarrow 4_2^+)$. The experimental data of this nucleus are typical of all open shell nuclei with

both valence protons and neutrons, namely, that the first value is much larger than the second one. However, the calculations for both interactions give at the $t = 0$ and $t = 2$ level the reverse results. For $t = 4$ and beyond we get the correct behavior for GXPF1 but not for FPD6. With GXPF1(10) we get excellent agreement for $B(E2; 0_1^+ \rightarrow 2_1^+)$ [0.1307 versus the experimental value of 0.130(9); see Table III]. That theory somewhat overpredicts the next collective transition, $B(E2; 2_1^+ \rightarrow 4_1^+)$ [0.0676 versus 0.040(3)]. The interaction also correctly predicts that the non-collective transition matrix elements are small, but because they are so small, it is hard to get them just right. The main discrepancy with GXPF1(10) is in the collective transition $B(E2; 4_1^+ \rightarrow 6_1^+)$, where the theoretical value is much too large [0.0758 versus 0.029(8)]. The problem may be that there are two 6^+ states with a small separation energy. That particular transition is predicted well by FPD6(10) [0.0317 versus 0.029(8)].

We have not included in our shell model space the $g_{9/2}$ orbital, which is known to be important in this mass region [1,2,7], especially for the higher spin states.

Furthermore, we have also considered the quadrupole moment of the 2_1^+ state in ^{68}Ge although it has not been measured yet. With both GXPF1(4) and FPD6(4) positive quadrupole moments are obtained for the $2_1^+, 4_1^+$, and 6_1^+ states, indicating oblate deformations. From the 2_1^+ calculated quadrupole moments we deduce an intrinsic quadrupole moment of $Q_\circ = -0.403$ b with GXPF1(4) and -1.61 b with FPD6(4). Raman *et al*. [24] deduce $|Q| = 1.20(9)$ from the measured $B(E2; 0_1^+ \rightarrow 2_1^+)$, closer to the FPD6(4) result.

Early shell model calculations by de Vries *et al*. [19] and Guilbault *et al*. [25] were similar to ours but less successful in reproducing the experimental data. This may have been due to the use of a simpler interaction, nucleon configuration truncations, and/or the extension to higher excitation energies.

IV. SUMMARY

In ^{68}Ge the $g(2_1^+)$ and some lifetimes have been measured using α transfer from a ^{12}C target to fast-moving ^{64}Zn projectiles. The α-transfer reaction is shown to be an important alternative to the spectroscopy of low-intensity radioactive ion beams.

The properties of the low-lying states of ^{68}Ge can be explained on the basis of a vibrational picture. However, the amount of collectivity and the low-energy structure of this nucleus are also well accounted for by extensive fp shell model calculations including the excitation of up to four nucleons from the $f_{7/2}$ orbital of the ^{56}Ni core. No evidence is found for shell closures at $N = 32$ or $Z = 32$. The $g_{9/2}$ intruder orbital does not seem to play a major role in the low-lying and low-spin structure of ^{68}Ge. To explain the measured $B(E2)$ values it is preferable to have ^{40}Ca rather than ^{56}Ni as the closed shell model core.

[1] M. Honma, T. Otsuka, B. A. Brown, and T. Mizusaki, Phys. Rev. C **65**, 061301(R) (2002).

[2] M. Honma, T. Otsuka, B. A. Brown, and T. Mizusaki, Phys. Rev. C **69**, 034335 (2004).

[3] O. Kenn, K.-H. Speidel, R. Ernst, J. Gerber, N. Benczer-Koller, G. Kumbartzki, P. Maier-Komor, and F. Nowacki, Phys. Rev. C **63**, 021302(R) (2000).

[4] O. Kenn, K.-H. Speidel, R. Ernst, J. Gerber, P. Maier-Komor, and F. Nowacki, Phys. Rev. C **63**, 064306 (2001).

[5] T. Otsuka, M. Honma, T. Mizusaki, N. Shimizu, and Y. Utsuno, Prog. Part. Nucl. Phys. **47**, 319 (2001).

[6] O. Kenn, K.-H. Speidel, R. Ernst, S. Schielke, S. Wagner, J. Gerber, P. Maier-Komor, and F. Nowacki, Phys. Rev. C **65**, 034308 (2002).

[7] J. Leske, K.-H. Speidel, S. Schielke, O. Kenn, D. Hohn, J. Gerber, and P. Maier-Komor, Phys. Rev. C **71**, 034303 (2005).

[8] D. Ward *et al*., Phys. Rev. C **63**, 014301 (2001), and refs. therein.

[9] S. Schielke, K.-H. Speidel, O. Kenn, J. Leske, N. Gemein, M. Offer, Y. Y. Sharon, L. Zamick, J. Gerber, and P. Maier-Komor, Phys. Lett. **B567**, 153 (2003).

[10] P. Maier-Komor, K.-H. Speidel, and A. Stolarz, Nucl. Instrum. Methods Phys. Res. A **334**, 191 (1993).

[11] C. Kittel, *Introduction to Solid State Physics* (Wiley, New York, 1976).

[12] T. W. Burrows, Nucl. Data Sheets **97**, 1 (2002).

[13] K.-H. Speidel *et al*., Phys. Rev. C **57**, 2181 (1998).

[14] J. C. Wells and N. R. Johnson, computer code LINESHAPE, ORNL, 1976.

[15] F. J. Ziegler, J. Biersack, and U. Littmark, *The Stopping and Range of Ions in Solids* (Pergamon, Oxford, 1985), Vol. 1.

[16] P. Raghavan, At. Data Nucl. Data Tables **42**, 189 (1989).

[17] K.-H. Speidel, O. Kenn, and F. Nowacki, Prog. Part. Nucl. Phys. **49**, 91 (2002).

[18] G. M. Gusinskii *et al*., Isv. Akad. Nauk SSSR **41**, 66 (1977).

[19] H. F. de Vries and P. J. Brussard, Z. Phys. A **286**, 1 (1978).

[20] A. P. de Lima *et al*., Phys. Rev. C **23**, 213 (1981).

[21] A. Etchegoyen *et al*., computer code OXBASH, MSU-NSCL Report No. 524, 1985 (unpublished).

[22] E. Caurier, computer code ANTOINE, Strasbourg, 1989.

[23] W. A. Richter, M. G. Van Der Merwe, R. E. Julies, and B. A. Brown, Nucl. Phys. **A523**, 325 (1991).

[24] S. Raman, C. W. Nestor, Jr., and P. Tikkanen, At. Data Nucl. Data Tables **78**, 1 (2001).

[25] F. Guilbault *et al*., Phys. Rev. C **15**, 894 (1977).